Iterative Sparse Maximum Likelihood-based Algorithms with Applications to SAR Imaging

Habti Abeida[1], Xianqi Li[2], Jian Li[3], Mosleh M. Al-Harthi[4]

[1, 2, 3] Department of Electrical and Computer Engineering, University of Florida, Gainesville, FL, 32611, USA

[4] Department of Electrical Engineering, University of Taif, Al-Haweiah, 21974, Saudi Arabia

[1]abeida3@yahoo.fr; [2]xianqili@ufl.edu; [3]li@dsp.ufl.edu; [4]mosleh2k@hotmail.com

***Abstract*- This paper presents a series of iterative sparse maximum likelihood-based approaches (SMLA) with applications to synthetic aperture radar (SAR) imaging. By using a particular form of Gaussian signal prior, iterative analytical expressions of the signal and noise power estimates are obtained by iteratively minimizing the stochastic maximum likelihood (SML) function with respect to only one scalar parameter at a time, resulting in power-based SMLA approaches. However, these power-based sparse approaches do not provide the phases of the unknown signals. To address this problem, a combined SMLA and Maximum A Posteriori (MAP) approach (referred to as the SMLA-MAP approach) for estimating the unknown complex-valued signals is proposed. The SMLA-MAP derivation is inspired by the sparse learning via iterative minimization (SLIM) approach, where a modified expression of the SLIM noise power estimation is proposed. We also show that SLIM can be viewed as a combination of the deterministic ML (DML) and iteratively re-weighted least squares (IRLS) approaches. Finally, numerical examples of SAR imaging using Slicy data, Backhoe data and Gotcha data are generated to compare the performances of the proposed and existing approaches .**

Keywords- Synthetic Aperture Radar (SAR); SAR Imaging; Sparse Signal Recovery; Maximum Likelihood (ML); Maximum A Posteriori (MAP); Sparse Learning via Iterative Minimization (SLIM); Iterative Adaptive Approach (IAA).

I. INTRODUCTION

Synthetic aperture radar (SAR) has been widely used in a variety of applications such as geosciences, remote sensing and defense [1]. SAR is an active sensor and has all-weather and day/night imaging capabilities. There are four distinct modes in which a SAR imaging system can operate: scan, stripmap, spotlight, and inverse SAR (ISAR). In this paper, we will mainly focus on the spotlight mode SAR. In spotlight mode SAR, the radar sensor steers its antenna beam to continuously illuminate the terrain patch being imaged. It can provide higher resolution than the stripmap and scan mode SAR, because it views a scene from multiple angles during a single pass [2].

There has been considerable interest recently in the use of SAR images in automated target recognition and decision-making tasks. The success of such tasks depends on how well the reconstructed SAR images exhibit certain features of the underlying scenes. Among the popular spotlight mode SAR image formation algorithms, the polar format algorithm (PFA) [1], is based on using interpolation and the Fourier transform. Another image reconstruction method, suggested by the tomographic formulation of SAR [4], is the filtered backprojection (FBP) algorithm [4, 5], where each radial slice in the Fourier space is considered as the one dimensional (1D) Fourier transform of the projection of the field at the corresponding angle. These data-independent algorithms suffer from important shortcomings, such as limited resolution, speckle, and sidelobe artifacts. Several data-adaptive algorithms have been considered for SAR imaging [6-10]. However, these approaches require a large number of data snapshots to provide accurate second-order statistics, which is hard to satisfy in practice.

Based on the observation that typical underlying signals of interest exhibit a degree of sparsity[1], Cetin *et al.* [11, 12] proposed a regularization model using ℓ_p-norm ($0 < p \le 1$) for enhancement of two dimensional (2D) spotlight mode SAR images in the complex-valued image domain. Kragh *et al.* [13] developed another regularized ℓ_p-norm based approach for SAR image restoration. These methods, however, like most existing sparse signal recovery algorithms, require the delicate choice of user parameters. A Bayesian maximum a posteriori (MAP) algorithm and a sparse learning via iterative minimization (SLIM) algorithm [15] have also been used for SAR imaging [21, 25]. MAP and SLIM are easy to use and are sparse signal recovery algorithms with excellent sidelobe suppression and high resolution properties. However, like many other sparse signal reconstruction algorithms, MAP and SLIM provide biased downward spectral estimates [25]. Moreover, although easy to choose, they have a user parameter as well.

Recently, a nonparametric and user parameter-free algorithm, referred to as the iterative adaptive approach (IAA) [22], was presented for applications including, for example, SAR imaging [20, 21, 25] and single-antenna radar systems [22]. The IAA algorithm provides accurate spectral estimates by iteratively updating the IAA covariance matrices, and produces SAR images with high resolution and relatively low sidelobes [21, 25]. Since IAA is computationally expensive, a fast implementation of IAA is developed in [23, 24] to improve its computational efficiency by exploiting the Toeplitz structure of the IAA covariance matrices. A regularized version of the IAA algorithm (IAA-R) is also developed in [20]. However, the images generated by IAA are dense while certain recognition and decision-making tasks may prefer more sparse images.

This work was supported in part by DoD under Grant No. HM1582-10- 1-0017 and NSF under Grant No. ECCS-0729727. The views and conclusions contained herein are those of the authors and should not be interpreted as necessarily representing the official policies or endorsements, either expressed or implied, of the U.S. Government. The U.S. Government is authorized to reproduce and distribute reprints for Governmental purposes notwithstanding any copyright notation thereon.

* Please address all correspondence to Habti Abeida. Phone:(966) 583367467; abeida3@yahoo.fr.

[1]This means that in an appropriate basis, they can be expressed in terms of a small number of nonzero coefficients.

In this paper, we first present a series of user parameter-free iterative sparse maximum likelihood-based algorithms (SMLA) for estimating the sparse signal powers and noise power. We then propose a complex-valued SMLA-MAP approach, which can not only provide accurate spectral estimation, but also give rise to sparse SAR images with high resolution and low sidelobe level properties. In Section II, we present briefly the complex-valued SAR signal model. In Section III, by using a particular form of Gaussian signal prior, iterative analytical expressions of the signal and noise power estimates are derived. In Section IV, we develop several versions of sparse power-based SMLA algorithms. Since the power estimates do not contain any information on the phases of the unknown signals, in Section V, a combined SMLA and MAP approach (referred to as the SMLA-MAP approach) is proposed to estimate the unknown complex-valued signals. The SMLA-MAP derivation is inspired by the SLIM approach, and a modified expression of the SLIM noise power estimation is proposed. We also show that the SLIM algorithm can be viewed as a combination of the DML and IRLS approaches. In Section VI, numerical examples of SAR imaging are generated to compare the performances of the proposed and existing approaches, particularly, the well-known CoSaMP (Compressive Sampling Matching Pursuit) [14]. Finally, conclusions are given in Section VII.

The following notations are used throughout the paper. Matrices and vectors are represented by bold upper and lower case characters, respectively. Vectors are by default in column orientation, while superscript T, H and $*$ stand for transpose, conjugate transpose and complex conjugate, respectively. $\mathrm{E}(\cdot)$, $\mathrm{Tr}(\cdot)$ and $\det(\cdot)$ are the expectation, trace and determinant operators, $vec(\cdot)$ is the ''vectorization'' operator that turns a matrix into a vector by stacking the columns of a matrix on top of each other, $\otimes$ denotes the Kronecker matrix product, $\mathbf{I}$ is the identity matrix, and $\mathbf{u}_m$ denotes the mth column of $\mathbf{I}$.

II. PROPLEM FORMULATION

The phase history data used to form complex-valued SAR images can in general be expressed as (e.g., [1, 11])

$$\mathbf{y} = \mathbf{A}\mathbf{x} + \mathbf{e}, \tag{1}$$

where $\mathbf{y} \in \mathrm{C}^M$ is a vector of measurements after appropriate pre-processing, $\mathbf{e}$ is a complex-valued Gaussian noise vector, $\mathbf{x} \in \mathrm{C}^K$ is the underlying scene reflectivity (the pixels in a scene form a vector), and $\mathbf{A} \in C^{M\times K}$ is a rank deficient $(M << K)$ ''sensing matrix''.

We assume that the components of the noise vector e are independent, zero-mean complex Gaussian random variables with unknown variance σ. We also assume that e and x are independent, and $\mathbf{P} \overset{\text{def}}{=} \mathrm{Diag}(\mathbf{p})$, where $\mathbf{p} \overset{def}{=} [p_1,\ldots,p_K]^T$ is the signal power vector. The covariance matrix of y that contains information about the unknown parameters $\mathbf{p}$ and σ is given by

$$\mathbf{R} \overset{\text{def}}{=} \mathbf{A}\mathbf{P}\mathbf{A}^{\mathrm{H}} + \sigma\mathbf{I}.$$

To form SAR images, we need to estimate the sparse vector $\mathbf{x}$ from $\mathbf{y}$. The most straightforward method is to perform the inverse Fourier transform, which gives the conventional delay-and-sum (DAS) or matched filtering approach [28]. However, the quality of the DAS image is usually unsatisfactory due to the low resolution and high sidelobe problems. In this paper, we first propose power-based iterative sparse SMLA approaches for estimating $\mathbf{p}$ and σ. Owing to the complex-valued and potentially random phase nature of the reflectivities in SAR images, we then derive a SMLA-MAP approach that combines the SMLA and MAP approaches for estimating the unknown complex-valued signals $\mathbf{x}$. We note that the approaches presented in this paper can also be applied to many applications requiring sparse signal recovery techniques.

III. STOCHASTIC ML APPROACH

In this section, we derive iterative analytical expressions of the signal and noise power estimates obtained by iteratively minimizing the stochastic maximum likelihood (SML) function with respect to only one scalar parameter at a time. Based on these expressions, we propose in Section IV the power-based SMLA approaches.

Suppose $\mathbf{x}$ and $\mathbf{e}$ are circularly Gaussian distributed, and $\mathbf{y}$ has a circular Gaussian distribution with zero-mean and covariance matrix $\mathbf{R}$. Thus, the stochastic negative log-likelihood function of $\mathbf{y}$ can be expressed as

$$L_{\mathrm{SML}}(\mathbf{p},\sigma) = \mathbf{y}^{\mathrm{H}}\mathbf{R}^{-1}\mathbf{y} + \ln(\det(\mathbf{R})). \tag{2}$$

Note that the first term in (2) is a convex function of $\mathbf{p}$ and σ. However, the second term in (2) can be shown to be a concave function of $\mathbf{p}$ and σ [27, Theorem 1]. Consequently, (2) is a non-convex function of $\mathbf{p}$ and σ. Despite this difficulty, we prove (see Appendix A) the following result.

Result 1. The $\{\hat{p}_k\}_{k=1}^K$ and $\hat{\sigma}$ that minimize (2) can be computed iteratively. Assume $\hat{p}_k^{(i)}$ and $\hat{\sigma}^{(\mathrm{i})}$ have been obtained in the *ith* iteration, they can be updated at the *(i+1)th* iteration as:

$$\hat{\mathrm{p}}_{\mathrm{k}}^{(\mathrm{i}+1)} = \frac{|\mathbf{a}_{\mathrm{k}}^{\mathrm{H}}\mathbf{R}^{-1(\mathrm{i})}\mathbf{y}|^2}{(\mathbf{a}_{\mathrm{k}}^{\mathrm{H}}\mathbf{R}^{-1(\mathrm{i})}\mathbf{a}_{\mathrm{k}})^2} + \hat{\mathrm{p}}_{\mathrm{k}}^{(\mathrm{i})} - \frac{1}{\mathbf{a}_{\mathrm{k}}^{\mathrm{H}}\mathbf{R}^{-1(\mathrm{i})}\mathbf{a}_{\mathrm{k}}}, \quad \mathrm{k}=1,\ldots,\mathrm{K}, \tag{3}$$

$$\hat{\sigma}^{(\mathrm{i}+1)} = \left(\mathbf{y}^{\mathrm{H}}\mathbf{R}^{-2(\mathrm{i})}\mathbf{y} + \hat{\sigma}^{(\mathrm{i})}\mathrm{Tr}(\mathbf{R}^{-2(\mathrm{i})}) - \mathrm{Tr}(\mathbf{R}^{-1(\mathrm{i})})\right)/\mathrm{Tr}(\mathbf{R}^{-2(\mathrm{i})}), \tag{4}$$

where the matrix $\mathbf{R}$ can be updated for each iteration as $\mathbf{R}^{(\mathrm{i})} = \mathbf{A}\mathbf{P}^{(\mathrm{i})}\mathbf{A}^{\mathrm{H}} + \hat{\sigma}^{(\mathrm{i})}\mathbf{I}$ and where $\mathbf{P}^{(\mathrm{i})} = \mathrm{Diag}(\hat{\mathrm{p}}_1^{(\mathrm{i})},\ldots,\hat{\mathrm{p}}_{\mathrm{K}}^{(\mathrm{i})})$.

Through numerical calculations, we have observed that the $\{\hat{p}_k\}_{k=1}^K$ and $\hat{\sigma}$ given by (3) and (4) may be negative; therefore, the nonnegativity of the power estimates can be enforced at each iteration by setting the negative estimates to zero as [22, Eq. (30)],

$$\begin{aligned} \hat{\mathrm{p}}_{\mathrm{k}}^{(\mathrm{i}+1)} &= \max\left(0, \mathrm{c}_{\mathrm{k}}^{(\mathrm{i}+1)}\right), \quad \mathrm{k}=1,\ldots,\mathrm{K}, \\ \hat{\sigma}^{(\mathrm{i}+1)} &= \max\left(0, \bar{\sigma}^{(\mathrm{i}+1)}\right), \end{aligned} \tag{5}$$

where $\mathrm{c}_{\mathrm{k}}^{(\mathrm{i}+1)} = \dfrac{|\mathbf{a}_{\mathrm{k}}^{\mathrm{H}}\mathbf{R}^{-1(\mathrm{i})}\mathbf{y}|^2}{(\mathbf{a}_{\mathrm{k}}^{\mathrm{H}}\mathbf{R}^{-1(\mathrm{i})}\mathbf{a}_{\mathrm{k}})^2} + \hat{\mathrm{p}}_{\mathrm{k}}^{(\mathrm{i})} - \dfrac{1}{\mathbf{a}_{\mathrm{k}}^{\mathrm{H}}\mathbf{R}^{-1(\mathrm{i})}\mathbf{a}_{\mathrm{k}}}$ and

$$\bar{\sigma}^{(\mathrm{i}+1)} = \left(\mathbf{y}^{\mathrm{H}}\mathbf{R}^{-2(\mathrm{i})}\mathbf{y} + \hat{\sigma}^{(\mathrm{i})}\mathrm{Tr}(\mathbf{R}^{-2(\mathrm{i})}) - \mathrm{Tr}(\mathbf{R}^{-1(\mathrm{i})})\right)/\mathrm{Tr}(\mathbf{R}^{-2(\mathrm{i})}).$$

The initialization of $\hat{p}_k$, $k=1,\ldots,K$, can be done with the power estimates obtained by means of the delay-and-sum (DAS) (or matched filtering) approach, (see, e.g., [28])

$$\hat{\mathbf{p}}_{k,\mathrm{DAS}}^{(0)} = \frac{|\mathbf{a}_k^{\mathrm{H}}\mathbf{y}|^2}{\|\mathbf{a}_k\|^4}, \quad k=1,\ldots,K. \tag{6}$$

The parameter $\hat{\sigma}$ can be initialized for instance as

$$\hat{\sigma}^{(0)} = \frac{1}{M}\|\mathbf{y}\|^2. \tag{7}$$

Remark 1. We note that Result 1 can be extended easily to the nonuniform white Gaussian noise case where the covariance matrix is given by

$$\mathrm{E}(\mathbf{e}(n)\mathbf{e}^{\mathrm{H}}(n)) = \mathrm{Diag}(\sigma_1,\ldots,\sigma_M) \overset{\mathrm{def}}{=} \sum_{m=1}^{M}\sigma_m \mathbf{a}_{K+m}\mathbf{a}_{K+m}^{\mathrm{T}}, \tag{8}$$

with $\mathbf{a}_{K+m} \overset{\mathrm{def}}{=} \mathbf{u}_m$, $m=1,\ldots,M$, denoting the canonical vector with one on its *mth* entry and zeros elsewhere. Under this assumption and from Result 1, the *(i+1)th* estimate of p_k, k=1,…,K+M, is given by

$$\hat{\mathrm{p}}_k^{(i+1)} = \frac{|\mathbf{a}_k^{\mathrm{H}}\mathbf{R}^{-1(i)}\mathbf{y}|^2}{(\mathbf{a}_k^{\mathrm{H}}\mathbf{R}^{-1(i)}\mathbf{a}_k)^2} + \hat{\mathrm{p}}_k^{(i)} - \frac{1}{\mathbf{a}_k^{\mathrm{H}}\mathbf{R}^{-1(i)}\mathbf{a}_k},$$

where $\mathbf{R}^{(i)} = \mathbf{A}\mathbf{P}^{(i)}\mathbf{A}^{\mathrm{H}} + \sum_{k=K+1}^{K+M}\hat{\sigma}_k^{(i)}\mathbf{a}_k\mathbf{a}_k^{\mathrm{T}}$ and where $\mathbf{P}^{(i)} = \mathrm{Diag}(\hat{\mathrm{p}}_1^{(i)},\ldots,\hat{\mathrm{p}}_K^{(i)})$ and $\hat{\sigma}_k^{(i)} = \hat{\mathrm{p}}_k^{(i)}$, $k=K+1,\ldots,K+M$.

IV. SMLA APPROACHES

As mentioned in Section III, Equations (3) and (4) may give negative power estiamtes in the overcomplete basis case due to the presence of non-zero terms $\mathrm{p}_k - 1/(\mathbf{a}_k^{\mathrm{H}}\mathbf{R}^{-1}\mathbf{a}_k)$ and $\sigma - \mathrm{Tr}(\mathbf{R}^{-1})/\mathrm{Tr}(\mathbf{R}^{-2})$. To alleviates this difficulty, we assume that[2] $\mathrm{p}_k = 1/(\mathbf{a}_k^{\mathrm{H}}\mathbf{R}^{-1}\mathbf{a}_k)$ and $\sigma = \mathrm{Tr}(\mathbf{R}^{-1})/\mathrm{Tr}(\mathbf{R}^{-2})$, and based on Result 1, we propose the following iterative power-based SMLA approaches. At the *(i+1)*th iteration, the signal and noise power estimates are computed based on the previous iterations.

A. SMLA-0 Approach

The estimates of $\{p_k\}_{k=1}^K$ and σ are updated at the *(i+1)*th iteration as:

$$\hat{\mathrm{p}}_k^{(i+1)} = \hat{\mathrm{p}}_k^{2(i)}(|\mathbf{a}_k^{\mathrm{H}}\mathbf{R}^{-1(i)}\mathbf{y}|^2), \quad k=1,\ldots,K, \tag{9}$$

$$\hat{\sigma}^{(i+1)} = \frac{\mathbf{y}^{\mathrm{H}}\mathbf{R}^{-2(i)}\mathbf{y}}{\mathrm{Tr}(\mathbf{R}^{-2(i)})}. \tag{10}$$

B. SMLA-1 Approach

The estimates of $\{p_k\}_{k=1}^K$ and σ are updated at the *(i+1)*th iteration as:

$$\hat{\mathrm{p}}_k^{(i+1)} = \frac{|\mathbf{a}_k^{\mathrm{H}}\mathbf{R}^{-1(i)}\mathbf{y}|^2}{(\mathbf{a}_k^{\mathrm{H}}\mathbf{R}^{-1(i)}\mathbf{a}_k)^2}, \quad k=1,\ldots,K, \tag{11}$$

$$\hat{\sigma}^{(i+1)} = \frac{\mathbf{y}^{\mathrm{H}}\mathbf{R}^{-2(i)}\mathbf{y}}{\mathrm{Tr}(\mathbf{R}^{-2(i)})}. \tag{12}$$

C. SMLA-2 Approach

The estimates of $\{p_k\}_{k=1}^K$ and σ are updated at the *(i+1)*th iteration as:

$$\hat{\mathrm{p}}_k^{(i+1)} = \hat{\mathrm{p}}_k^{(i)}\frac{|\mathbf{a}_k^{\mathrm{H}}\mathbf{R}^{-1(i)}\mathbf{y}|^2}{\mathbf{a}_k^{\mathrm{H}}\mathbf{R}^{-1(i)}\mathbf{a}_k}, \quad k=1,\ldots,K, \tag{13}$$

$$\hat{\sigma}^{(i+1)} = \frac{\mathbf{y}^{\mathrm{H}}\mathbf{R}^{-2(i)}\mathbf{y}}{\mathrm{Tr}(\mathbf{R}^{-2(i)})}.$$

D. SMLA-3 Approach:

The estimates of $\{p_k\}_{k=1}^K$ and σ are updated at the *(i+1)*th iteration as:

$$\hat{\mathrm{p}}_k^{(i+1)} = \frac{|\mathbf{a}_k^{\mathrm{H}}\mathbf{R}_1^{-1(i)}\mathbf{y}|^2}{(\mathbf{a}_k^{\mathrm{H}}\mathbf{R}^{-1(i)}\mathbf{a}_k)^2}, \quad k=1,\ldots,K, \tag{14}$$

$$\hat{\sigma}^{(i+1)} = \frac{\mathbf{y}^{\mathrm{H}}\mathbf{R}^{-2(i)}\mathbf{y}}{\mathrm{Tr}(\mathbf{R}^{-2(i)})}.$$

where $\mathbf{R}_1^{(i)} = \mathbf{A}\mathbf{P}_1^{(i)}\mathbf{A}^{\mathrm{H}} + \sigma^{(i)}\mathbf{I}$ and $\mathbf{P}_1^{(i)} = \mathrm{Diag}(\hat{\mathrm{p}}_1^{(i)},\ldots,\hat{\mathrm{p}}_K^{(i)})$, with $\hat{\mathrm{p}}_k^{(i)} = \frac{1}{\mathbf{a}_k^{\mathrm{H}}\mathbf{R}^{-1(i)}\mathbf{a}_k}$, $k=1,\ldots,K$.

In the special case of nonuniform white Gaussian noise with covariance matrix given in Remark 2, the SMLA noise power estimates must be updated at each iteration as

$$\hat{\sigma}_m^{(i+1)} = \frac{|\mathbf{u}_m^{\mathrm{H}}\mathbf{R}^{-1(i)}\mathbf{y}|^2}{(\mathbf{u}_m^{\mathrm{H}}\mathbf{R}^{-1(i)}\mathbf{u}_m)^2}, \quad m=1,\ldots,M, \tag{15}$$

where $\mathbf{R}^{(i)} = \mathbf{A}\mathbf{P}^{(i)}\mathbf{A}^{\mathrm{H}} + \sum_{m=1}^{M}\hat{\sigma}_m^{(i)}\mathbf{u}_m\mathbf{u}_m^{\mathrm{T}}$ and where $\mathbf{P}^{(i)} = \mathrm{Diag}(\hat{\mathrm{p}}_1^{(i)},\ldots,\hat{\mathrm{p}}_K^{(i)})$.

In the following result (proved in Appendix B), we show that the SMLA-1 signal and noise power-iterations given by (11) and (12) can be obtained by minimizing a weighted least squares (WLS) cost function.

Result 2. The SMLA-1 estimates coincide with the estimates $\hat{p}_k$ and $\hat{\sigma}$ obtained by minimizing the following WLS cost function

$$\hat{\mathrm{p}}_k = \arg\min_{\mathrm{p}_k} \mathrm{g}(\mathrm{p}_k) \overset{\mathrm{def}}{=} [\mathbf{r}_y - \mathrm{p}_k\mathbf{a}_k]^{\mathrm{H}}\mathbf{C}_k^{-1}[\mathbf{r}_y - \mathrm{p}_k\mathbf{a}_k]. \tag{16}$$

[2]The term $\mathrm{p}_k = 1/(\mathbf{a}_k^{\mathrm{H}}\mathbf{R}^{-1}\mathbf{a}_k)$ is the estimate of the *k*-th power component given by the Capon estimator [28].

where $\mathbf{r}_y \overset{\text{def}}{=} \mathbf{y}^* \otimes \mathbf{y}$ and $\mathbf{C}'_k \overset{\text{def}}{=} \mathbf{C}_r - p_k^2 \mathbf{a}_k \mathbf{a}_k^H$, $k = 1, \ldots, K+1$, with $\mathbf{C}_r \overset{\text{def}}{=} \mathbf{R}^* \otimes \mathbf{R}$.

The implementation steps of these approaches are summarized in Table Ⅰ.

TABLE Ⅰ THE SMLA APPROACHES

Initialization: $p^{(0)}$ and $\sigma^{(0)}$ using e.g., (6) and (7)
Repeat • Update $\mathbf{R}^{(i)} = \mathbf{A}\mathbf{P}^{(i)}\mathbf{A}^H + \sigma^{(i)}\mathbf{I}$ or $\mathbf{R}_1^{(i)} = \mathbf{A}\mathbf{P}_1^{(i)}\mathbf{A}^H + \sigma^{(i)}\mathbf{I}$. • Update $p_k^{(i+1)}$ using SMLA identities (9), (11), (14), or (13). • Update $\sigma^{(i+1)}$ using (12).

Remark 2. *Note that the SMLA-0 power estimate expression (9) can be interpreted as*

$$\hat{p}_{k,SMLA-0} = |\hat{x}_{k,MAP}|^2, \quad k = 1, \ldots, K,$$

where $\hat{x}_{k,MAP} = p_k \mathbf{a}_k^H \mathbf{R}^{-1} \mathbf{y}$ is the maximum a posterior (MAP) estimate (Eq. (25)) of x_k, $k = 1, \ldots, K$.

Comparing SMLA-1 power estimate expression (11) and that associated with the IAA approach ([22, Table II]), we see that the difference between SMLA-1 and IAA is that the IAA power estimate is obtained after the estimation of the magnitude of $\{x_k\}_{k=1}^K$ (i.e., $\hat{p}_{k,IAA} = |\hat{x}_{k,IAA}|^2$), by updating the IAA covariance matrix $\mathbf{A}\mathbf{P}\mathbf{A}^H$ for each iteration.

V. SMLA-MAP

The main purpose of this section is to derive the SMLA-MAP approach based on the power-based SMLA approaches presented in Section 4. Our derivation is inspired by the work of Wipf *et al.* [16, 17] and the derivation of the SLIM approach [15].

A. SLIM

In this section, we first recall briefly the main iteration steps of the SLIM approach [15]. We show that the SLIM approach can be viewed as a combination of the deterministic ML (DML) and iteratively re-weighted least squares (IRLS) approaches. We also quantify the classical SLIM estimate expression of the noise power by deriving a new expression that depends on the previous estimate of the signal power vector.

The SLIM approach is derived based on the following hierarchical Bayesian model [15]:

$$\mathbf{y} \mid \mathbf{x}, \sigma : N_c(\mathbf{A}\mathbf{x}, \sigma\mathbf{I}), \mathrm{f}_e(\sigma) \propto 1 \tag{17}$$

$$\mathrm{f}_q(\mathbf{x}) \overset{\text{def}}{=} \prod_{n=1}^{N} e^{-\frac{2}{q}(|x_n|^q - 1)}, \tag{18}$$

where $\mathrm{f}_q(\mathbf{x})$ is a sparsity-promoting prior for $0 < q \le 1$. Then, the SLIM estimates of $\mathbf{x}$ and σ are obtained by minimizing the following MAP criterion:

$$\{\hat{\mathbf{x}}, \hat{\sigma}\} = \arg\min_{\mathbf{x},\sigma} L_q(\mathbf{x}, \sigma) \overset{\text{def}}{=} -\log(\ell(\mathbf{y} \mid \mathbf{x}, \sigma)\mathrm{f}_q(\mathbf{x})\mathrm{f}_e(\sigma)). \tag{19}$$

Using (17) and (18), we have

$$L_q(\mathbf{x}, \sigma) \overset{\text{def}}{=} L^{\mathrm{DML}}(\mathbf{x}, \sigma) + \mathrm{L}_q^{\mathrm{Reg}}(\mathbf{x}),$$

where $\mathrm{L}^{\mathrm{DML}}(\mathbf{x}, \sigma)$ is the negative log-likelihood function for the deterministic ML approach:

$$L^{\mathrm{DML}}(\mathbf{x}, \sigma) \overset{\text{def}}{=} \mathrm{M}\log(\sigma) + \frac{1}{\sigma}\|\mathbf{y} - \mathbf{A}\mathbf{x}\|^2,$$

and the regularized function $\mathrm{L}_q^{\mathrm{Reg}}(\mathbf{x})$ is defined as the negative of the function $\mathrm{f}_q(\mathbf{x})$ given by

$$L_q^{\mathrm{Reg}}(\mathbf{x}) \overset{\text{def}}{=} -\log(\mathrm{f}_q(\mathbf{x})) = \frac{2}{q}\sum_{k=1}^{K}(|\mathrm{x}_k|^q - 1).$$

Minimizing (19) w.r.t. $\mathbf{x}$ is equivalent to minimizing w.r.t. $\mathbf{x}$ the following function

$$\frac{1}{\sigma}\|\mathbf{y} - \mathbf{A}\mathbf{x}\|^2 + \mathrm{L}_q^{\mathrm{Reg}}(\mathbf{x}) = \frac{1}{\sigma}\|\mathbf{y} - \mathbf{A}\mathbf{x}\|^2 + \frac{2}{q}\|\mathbf{x}\|_q^q - \frac{2K}{q}.$$

The solution is given by [15, Eq. (25)]

$$\mathbf{x}^{(i+1)} = \tilde{\mathbf{P}}^{(i)}\mathbf{A}^H\tilde{\mathbf{R}}^{-1(i)}\mathbf{y}, \tag{20}$$

with

$$\tilde{\mathbf{R}}^{(i)} \overset{\text{def}}{=} \mathbf{A}\tilde{\mathbf{P}}^{(i)}\mathbf{A}^H + \sigma^{(i)}\mathbf{I},$$

$$\tilde{\mathbf{P}}^{(i)} \overset{\text{def}}{=} \mathrm{Diag}(1/\tilde{\mathrm{p}}_1^{(i)}, \ldots, 1/\tilde{\mathrm{p}}_K^{(i)}) \text{ and } \tilde{p}_k^{(i)} = |x_k^{(i)}|^{q-2}.$$

Minimizing (19) w.r.t. σ is equivalent to minimizing the DML cost function $\mathrm{L}^{DML}(.)$ w.r.t. σ, and the solution is given by the following classical SLIM noise power estimate

$$\sigma^{(i+1)} = \frac{1}{\mathrm{M}}\|\mathbf{y} - \mathbf{A}\hat{\mathbf{x}}^{(i+1)}\|^2. \tag{21}$$

Therefore, by substituting $\mathrm{x}^{(i+1)}$ into (21), we obtain

$$\mathbf{y} - \mathbf{A}\hat{\mathbf{x}}^{(i+1)} = \mathbf{\Omega}\mathbf{y},$$

where

$$\mathbf{\Omega}^{(i+1)} \overset{\text{def}}{=} \mathbf{I} - (\mathbf{A}\mathbf{P}^{(i)}\mathbf{A}^H)\tilde{\mathbf{R}}^{-1(i)} = \sigma^{(i)}\tilde{\mathbf{R}}^{-1(i)}.$$

Then, the estimate of the noise power can be updated at each iteration using the following equation instead of (21):

$$\sigma^{(i+1)} = \sigma^{2(i)} \frac{\mathbf{y}^H \widetilde{\mathbf{R}}^{-2(i)} \mathbf{y}}{M}. \quad (22)$$

We note the expression given by (20) is the solution to the following ℓ_q optimization problem solved using the iterative re-weighted least-squares algorithm (IRLS) (e.g., [18])

$$\frac{1}{\sigma^{(i)}} \| \mathbf{y} - \mathbf{A}\mathbf{x} \|^2 + \sum_{k=1}^{K} \widetilde{p}_k^{(i)} | x_k |^2 = \frac{1}{\sigma^{(i)}} \| \mathbf{y} - \mathbf{A}\mathbf{x} \|^2 + \mathbf{x}^H \widetilde{\mathbf{P}}^{-1(i)} \mathbf{x}.$$

The matrix $\widetilde{\mathbf{P}}^{(i)}$ here can be viewed as the weighting matrix. Thus, the SLIM optimization problem (19) is equivalent to the following ℓ_q optimization problem

$$M \log(\sigma) + \frac{1}{\sigma} \| \mathbf{y} - \mathbf{A}\mathbf{x} \|^2 + \| \mathbf{x} \|_q^q,$$

and its solution is obtained by combing the deterministic ML approach to obtain (22) and the IRLS approach to obtain (20).

B. SMLA-MAP

We first recall that the SMLA approaches can be viewed as approximate solutions of the stochastic ML criterion by minimizing the cost function $L_{SML}(\cdot)$. Note also that the estimates of $\{p_k\}_{k=1}^K$ can be a good tool to determine whether $\{|x_k|\}_{k=1}^K$ are large or small, which is mainly required for signal detection applications. However, the powers $\{p_k\}_{k=1}^K$ do not contain any information on the phases of the complex-valued signals $\{x_k\}_{k=1}^K$ needed by some practical sparse signal recovery applications. Moreover, direct calculation of $\{|x_k|\}_{k=1}^K$ from $\{p_k\}_{k=1}^K$ may not always be possible due to some unknown scaling factor that is involved (see, e.g., [26]). To alleviate this difficulty, we describe here how to estimate the complex-valued signal $\mathbf{x}$ and the hyperparameters $\mathbf{p}$ and σ by combining a SMLA approach and the maximum a posteriori probability (MAP) approach, resulting in the SMLA-MAP method. We note that in the derivation of the SLIM approach, the hyperparameters σ and $\mathbf{x}$ are estimated by the DML and MAP approaches, respectively. Therefore, a question arises as well: how can we combine the SML and MAP approaches in order to take advantage of the approximate SMLA solution?

For the special case of Bayesian real-valued data model, Wipf *et al.* have recently proved [16, Theorem 1 and 2] that the estimate of x and the hyperparameters (only the signal powers are assumed unknown) can be obtained by minimizing an auxiliary cost function, constructed by relying on the MAP-based cost function (Type I in [16]) and SML cost function (Type II in [16]). Reminiscent of their approach (e.g., [16, 17]) and using the complex-valued data model (1), we propose the following auxiliary cost function

$$L(\mathbf{x}, \mathbf{p}, \sigma) = \frac{1}{\sigma} \| \mathbf{y} - \mathbf{A}\mathbf{x} \|^2 + \mathbf{x}^H \mathbf{P}^{-1} \mathbf{x} + \log(\det(\mathbf{R})). \quad (23)$$

We first assume that p and σ are fixed. Therefore, minimizing (23) w.r.t. x is equivalent to minimizing the following MAP-based cost function w.r.t. x:

$$\hat{\mathbf{x}} = \arg\min_{\mathbf{x}} L_{MAP}(\mathbf{x}) = \frac{1}{\sigma} \| \mathbf{y} - \mathbf{A}\mathbf{x} \|^2 + \mathbf{x}^H \mathbf{P}^{-1} \mathbf{x}. \quad (24)$$

The solution to (24) can be obtained explicitly as

$$\mathbf{x}_{MAP}(\mathbf{p}, \sigma) = \mathbf{P}\, \mathbf{A}^H \mathbf{R}^{-1} \mathbf{y}. \quad (25)$$

The next step is to minimize (23) w.r.t. $\mathbf{p}$ and σ with fixed x. First, inserting the solution $\hat{\mathbf{x}}(\mathbf{p}, \sigma)$ into (23) and using the following key equality (proved in Appendix C)

$$\frac{1}{\sigma} \| \mathbf{y} - \mathbf{A}\hat{\mathbf{x}}_{MAP} \|^2 + \hat{\mathbf{x}}_{MAP}^H \mathbf{P}^{-1} \hat{\mathbf{x}}_{MAP} = \mathbf{y}^H \mathbf{R}^{-1} \mathbf{y}, \quad (26)$$

the cost function (23) becomes the SML cost function

$$L_{SML}(\mathbf{p}, \sigma) = \mathbf{y}^H \mathbf{R}^{-1} \mathbf{y} + \log(\det(\mathbf{R})). \quad (27)$$

As we have shown in Section IV, the SMLA estimates of the parameters $\mathbf{p}$ and σ given by (9)-(13) and (12) can be seen as an approximate solution to the following minimization problem

$$\{\hat{\mathbf{p}}_{SMLA}, \hat{\sigma}_{SMLA}\} = \arg\min_{\mathbf{p}, \sigma} L_{SML}(\mathbf{p}, \sigma).$$

Hence once $\hat{\mathbf{p}}_{SMLA}$ and $\hat{\sigma}_{SMLA}$ are obtained (at convergence of a SMLA approach), and using (25), the final estimate of the unknown complex-valued signal x is given by

$$\hat{\mathbf{x}}_{MAP} \overset{def}{=} \hat{\mathbf{x}}_{MAP}(\hat{\mathbf{p}}_{SMLA}, \hat{\sigma}_{SMLA}) = \mathbf{P}_{SMLA} \mathbf{A}^H \mathbf{R}_{SMLA}^{-1} \mathbf{y},$$

where $\mathbf{R}_{SMLA} = \mathbf{A}\mathbf{P}_{SMLA}\mathbf{A}^H + \hat{\sigma}_{SMLA}\mathbf{I}_M$, with

$$\hat{\mathrm{P}}_{SMLA} = \mathrm{Diag}(\hat{\mathbf{p}}_{SMLA}).$$

Consequently, the following result is proved.

Result 3. *Given the final SMLA estimates* $\hat{\mathbf{p}}_{SMLA}$ *and* $\hat{\sigma}_{SMLA}$*, the MAP estimate of the complex-valued signal* x *is given by*

$$\hat{\mathbf{x}}_{MAP} = \mathbf{P}_{SMLA} \mathbf{A}^H \mathbf{R}_{SMLA}^{-1} \mathbf{y}. \quad (28)$$

From this result, the estimates of the coefficients x and the hyperparameters $\{\mathbf{p}, \sigma\}$ may be obtained in a separable form. Note also from (28) that if $\hat{\mathbf{p}}_{SMLA}$ is K_s – sparse[3], then $\hat{\mathrm{x}}_{MAP}$ is K_s – sparse, with nonzero elements corresponding with the 'relevant' basis vectors $\mathbf{a}_k$, $k = 1, \ldots, K_s$.

VI. NUMERICAL AND EXPERIMENTAL EXAMPLES

In this section, we present the results of the power-based SMLA algorithms and the complex-valued SMLA-MAP approaches on three SAR data sets: Slicy, Backhoe, and

3A vector is said to be if K_s – sparse if it has at most K_s nonzero enters.

Gotcha. To illustrate the enhanced performance, the proposed approaches are compared with the following existing methods: FFT, windowed FFT (WFFT), CoSaMP (the user parameter is set to be 3000) and SLIM (with $q = 1$). Unless otherwise specified, the number of iterations [4] is fixed at 10 for all iterative algorithms. Note that all images are shown in dB, $10\log_{10}$ for power and $20\log_{10}$ for modulus, normalized to peak at 0 dB and with a dynamic range of 35 dB.

A. SAR Images of the Slicy Data

We use the two-dimensional phase-history data of the Slicy target generated at azimuth angle 0° using XPATCH [19], a high frequency electromagnetic scattering prediction code for complex 3-D objects. A photo of the Slicy target at 30° rotation is shown in Fig. 1. For all obtained images, a 40×40 center block of the phase-history data is used.

Fig. 1 Photo of the Slicy object viewed at azimuth angle 45 °

In the first experiment, we show SAR images of the Slicy data using the power-based SMLA algorithms presented in Section IV. In the second experiment, we show the reconstructed Slicy images using the complex-valued SMLA-MAP algorithm (i.e., based on the estimates of the complex-valued signal) presented in Section V.

Fig. 2 illustrates the SAR image formed using the WFFT approach, where a 2-D Taylor window with a -30 dB sidelobe level is applied. We can observe that WFFT has low resolution.

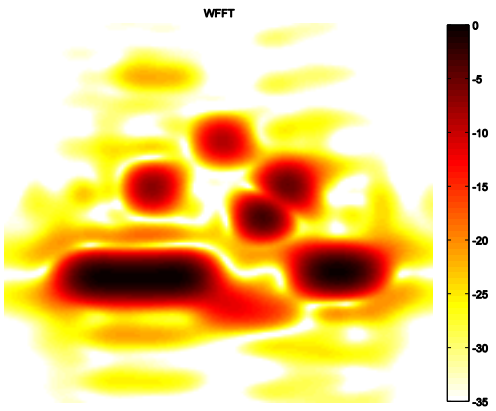

Fig. 2 2-D SAR image obtained via WFFT algorithm

Fig. 3 shows the SAR image obtained by CoSaMP, which fails to work properly since the object features are deteriorated.

4 In our simulations, we observe that there is no significant imaging quality improvement after 10 iterations.

In contrast, we can see from Fig. 4 that SMLA-0 with 3 iterations generates a SAR image with much higher resolution and lower sidelobes.

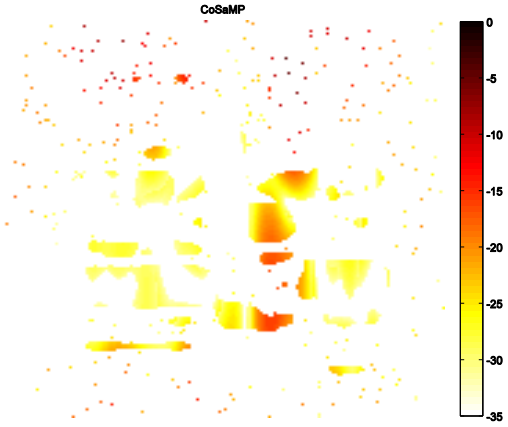

Fig. 3 2-D SAR image obtained via CoSaMP algorithm

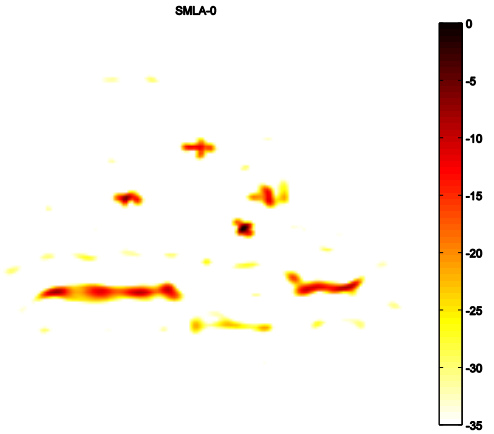

Fig. 4 2-D SAR image obtained via SMLA-0 algorithm (3 iterations)

Based on Remark 2, the performance of SMLA-1 and IAA are equivalent for high-SNR, where $\sigma \approx 0$. We observe from Fig. 5 that the reconstructed SAR image using the SMLA-1 approach has very high resolution with moderate sidelobe levels due to the fact that SMLA-1 is a dense algorithm.

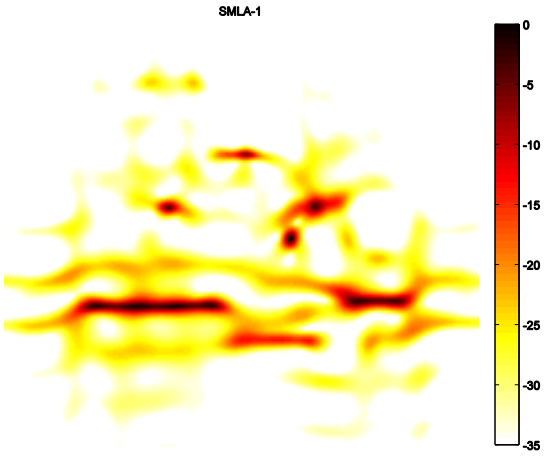

Fig. 5 2-D SAR image obtained via SMLA-1 algorithm.

Figs. 6 and 7 illustrate the imaging performance of the SMLA-2 and SMLA-3 approaches, respectively. As can be seen in Fig. 6, the SMLA-2 approach attenuates the sidelobe further compared with SMLA-1. We conclude that the SMLA-

2 approach is sparser than the SMLA-1 approach, and its performance is between those of SMLA-0 and SMLA-1. Similar to the SMLA-0 approach, the SAR image formed by the SMLA-2 approach is obtained with only 3 iterations. It can be concluded from Fig. 7 that the SMLA-3 approach produces the SAR image with the best appearance among these algorithms. However, this is for the noise-free case.

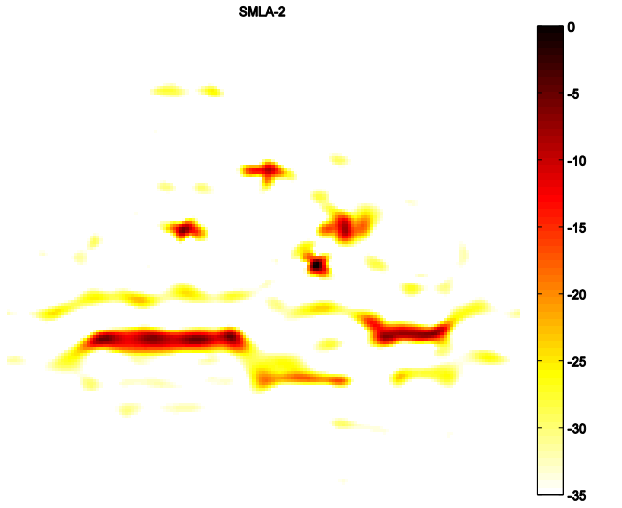

Fig. 6 2-D SAR image obtained via SMLA-2 algorithm (3 iterations)

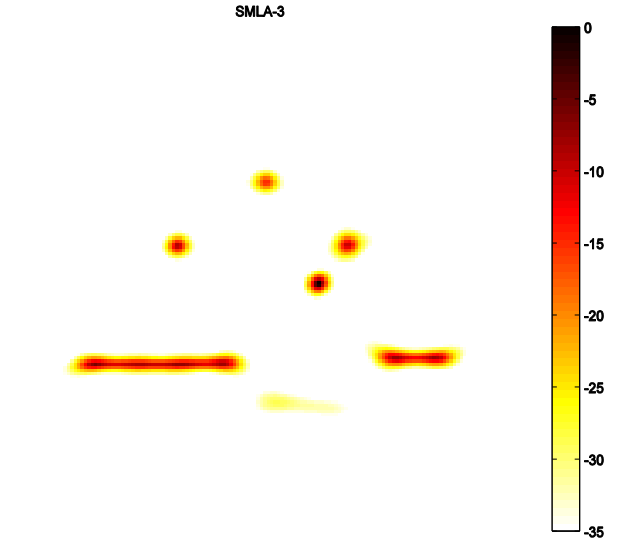

Fig. 7 2-D SAR image obtained via SMLA-3 algorithm

In the next example, we show in Fig. 8 the modulus of the complex-valued SAR image generated using the SLIM-1 approach (setting $q = 1$ in (20)). Figs. 9 and 10 demonstrate the performance of the proposed complex-valued SMLA-MAP approach given by Result 3. Figs. 9 and 10 show the modulus of the reconstructed SAR images using the complex-valued SMLA-1-MAP and SMLA-2-MAP approaches, respectively. In these figures, the estimates of the complex-valued signal $\mathbf{x}$ given by SMLA-1-MAP and SMLA-2-MAP were obtained using MAP and the SMLA-1 and SMLA-2 power estimates shown in Figs. 5 and 6, respectively. These figures demonstrate the effectiveness of these approaches in forming SAR images with enhanced resolution and suppressed sidelobes when compared to the power-based SMLA-1 and SMLA-2 approaches. They also show that the SLIM-1 approach is somewhat inferior to SMLA-1-MAP.

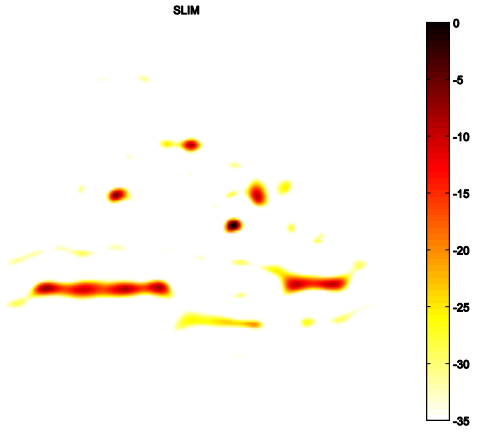

Fig. 8 2-D SAR image obtained via SLIM-1 algorithm

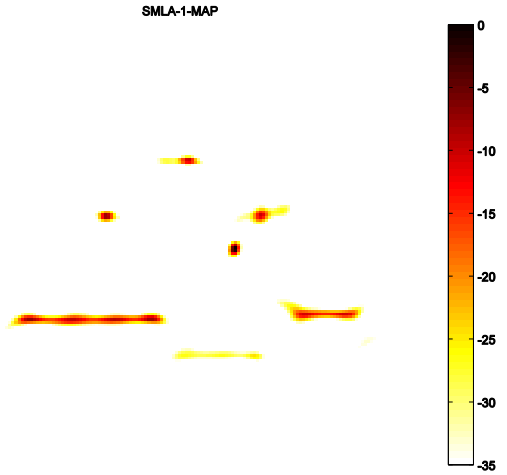

Fig. 9 2-D SAR image obtained via SMLA-1-MAP algorithm

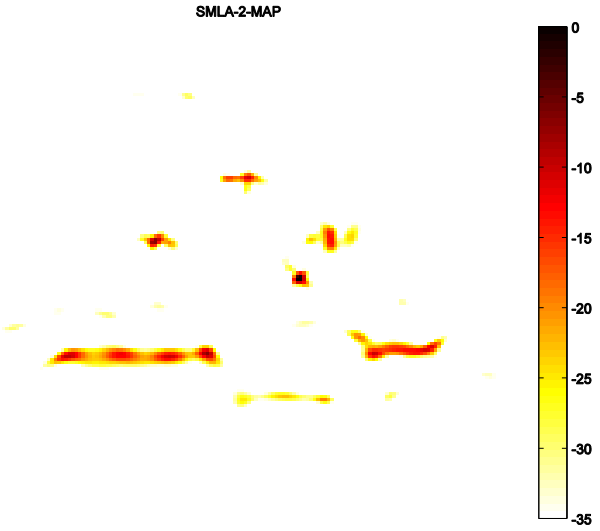

Fig. 10 2-D SAR image obtained via SMLA-2-MAP algorithm

In Fig. 11 we show the reconstructed image using SMLA-0 with 10 iterations, where the dominant powers are significantly accentuated. This phenomenon is ubiquitous among highly sparse algorithms. The reconstructed SMLA-2 image after 10 iterations is shown in Fig. 12. Fig. 13 shows the number of non-zero elements in $\mathbf{p}$, K_s, versus the iteration number. We remark from this figure that after 15 iterations the number of non-zero power elements decreases from 1.6×10^4 to 91 as the

number of iterations increases. Note that both SMLA-0 and SMLA-2 are too sparse after 10 iterations.

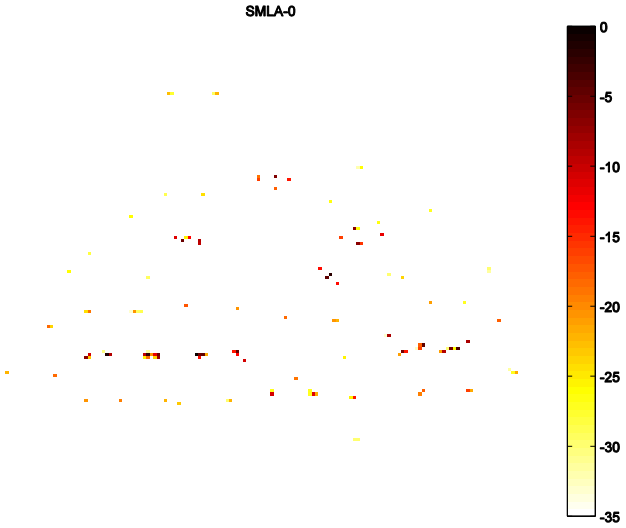

Fig. 11 2-D SAR image (power) obtained via SMLA-0 algorithm after convergence (using 10 iterations)

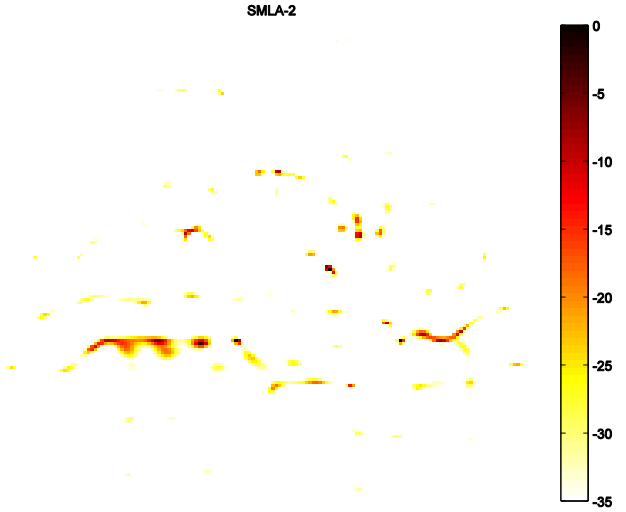

Fig. 12 2-D SAR image (power) obtained via SMLA-2 algorithm after convergence (using 10 iterations)

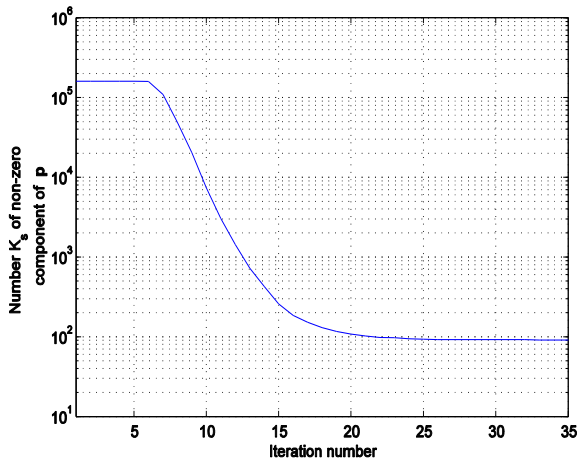

Fig. 13 The number, K_s of non-zero SMLA-0 power estimates versus the iteration number

To show the robustness of the proposed SMLA-MAP algorithms against the presence of noise, we consider further the case when the Slicy data is corrupted by white Gaussian noise with zero-mean and variance σ. Based on the data model (1), the SNR is defined as

$$\mathrm{SNR} \stackrel{\mathrm{def}}{=} \frac{\| \mathbf{Ax} \|^2}{\mathrm{M}\sigma}.$$

The SAR images given in Figs. 14-19 are formed with an SNR of 5 dB. As can be seen from Figs. 17 and 18, the SMLA-1-MAP and SMLA-2-MAP approaches provide better SAR images compared with the power-based SMLA-1 and SMLA-2 approaches illustrated by Figs. 14 and 15, resepectively. We can also see that SMLA-1-MAP produces a better image than SMLA-2-MAP. SMLA-3 and SMLA-3-MAP, shown in Figs. 16 and 19, respectively, appear to provide poorer images than their SMLA-1 counterparts for this noisy data case.

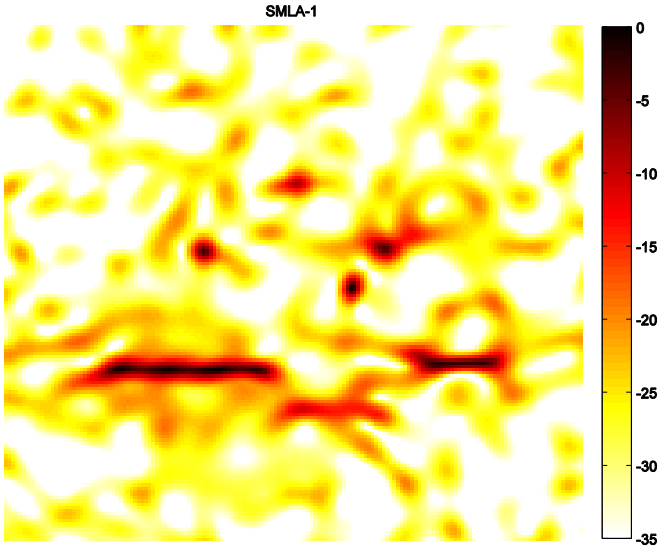

Fig. 14 2-D SAR image obtained from Slicy data with SNR=5 dB via SMLA-1 algorithm

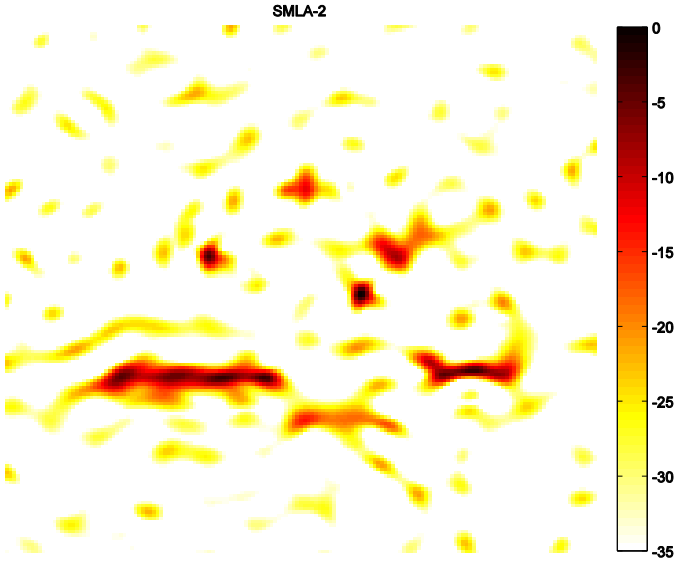

Fig. 15 2-D SAR image obtained from Slicy data with SNR=5 dB via SMLA-2 algorithm (3 iterations)

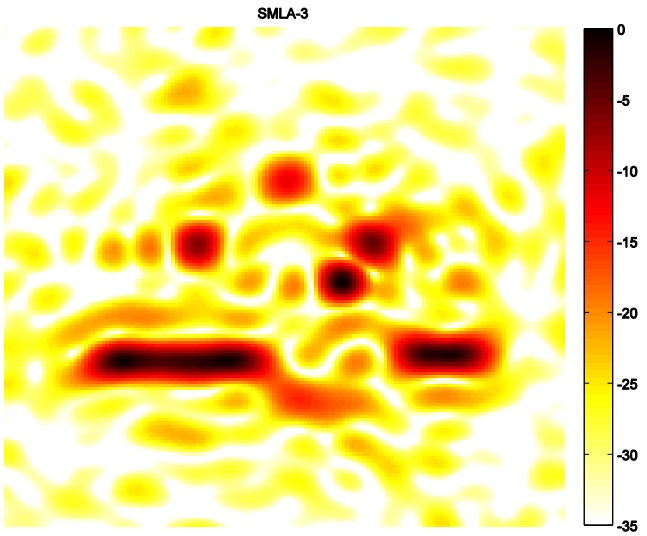

Fig. 16 2-D SAR image obtained from Slicy data with SNR=5 dB via SMLA-3 algorithm

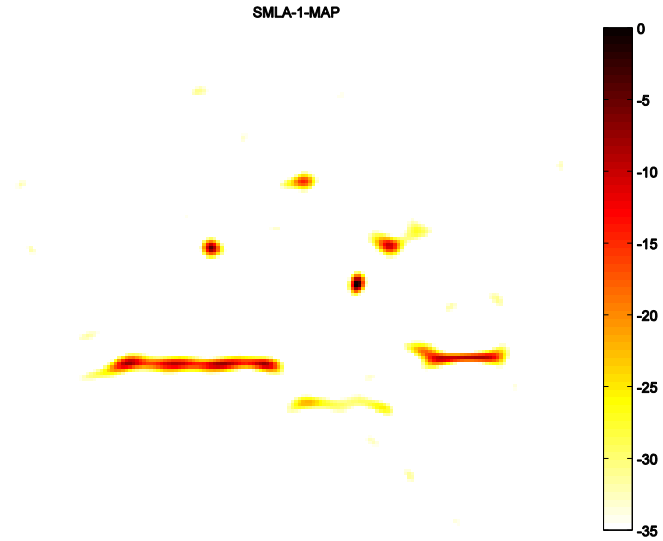

Fig. 17 2-D SAR image obtained from Slicy data with SNR=5 dB via SMLA-1-MAP algorithm

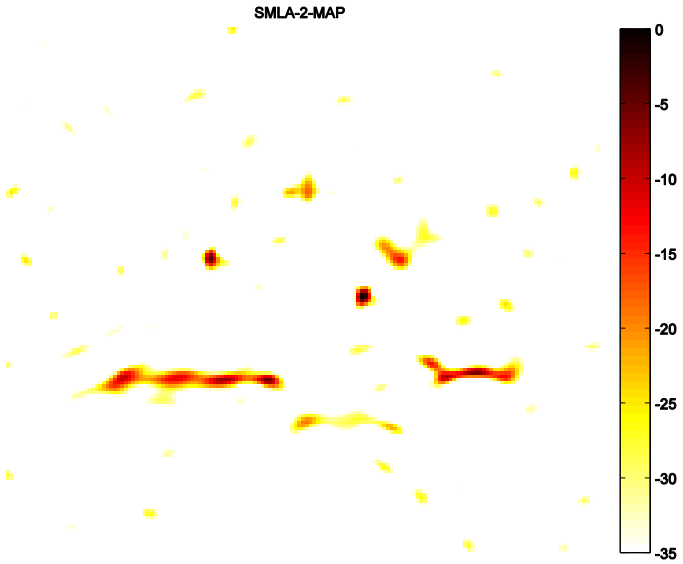

Fig. 18 2-D SAR image obtained from Slicy data with SNR=5 dB via SMLA-2-MAP algorithm (3 iterations)

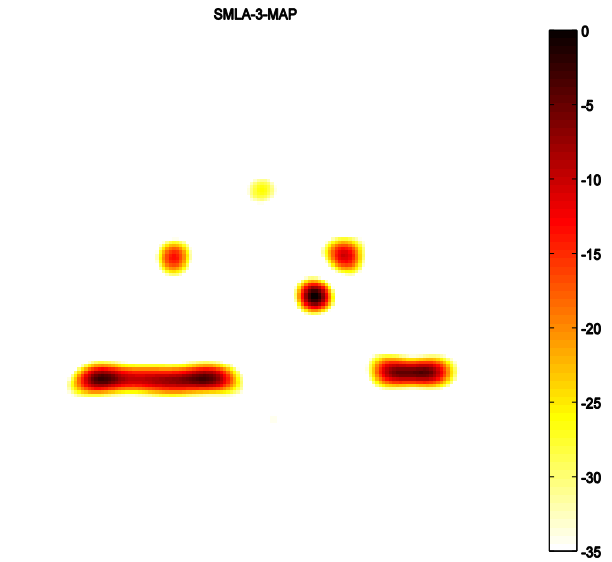

Fig. 19 2-D SAR image obtained from Slicy data with SNR=5 dB via SMLA-3-MAP algorithm

B. SAR Images of the Backhoe Data

In this subsection, we present numerical results using the Backhoe Data, which is a wideband, full polarization, complex-valued backscattered data from a backhoe vehicle in free space. Similarly, the Backhoe data is also corrupted by white Gaussian noise with zero--mean and variance σ. The 3-D CAD model of the backhoe and the illustration of the backhoe data dome are shown in Figs. 20-21. In our experiment, we use the 44×43 HH polarization data with a bandwidth of 0.5 GHz centered at 12 GHz. This data is collected at a 30° elevation angle and a 5° azimuth cut centered around 0° azimuth.

Fig. 20 The backhoe data: 3-D CAD model

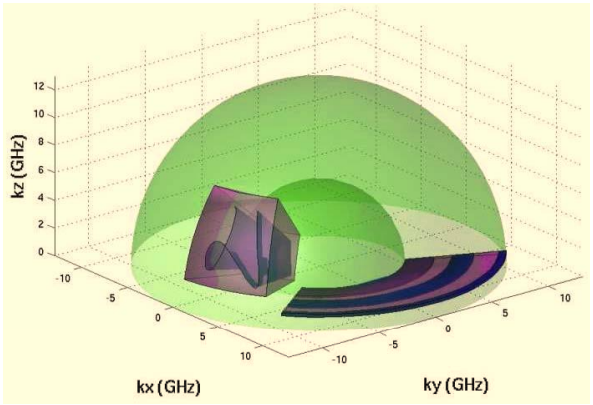

Fig. 21 The backhoe data: K-space data

With the same definition of SNR as for the Slicy data, the SAR images obtained using Backhoe data are given in Figs. 22-25 when the SNR is 5 dB. Fig. 22 shows the reconstructed SAR image obtained using the FFT approach. We can see from this figure that it has poor resolution and high sidelobe level problems. Fig. 23 shows the reconstructed image using the CoSaMP, which lacks fidelity. Figs. 24-25 illustrate the imaging performance of the SMLA-1 and SMLA-1-MAP approaches. Again, SMLA-1-MAP appears to give the best performance.

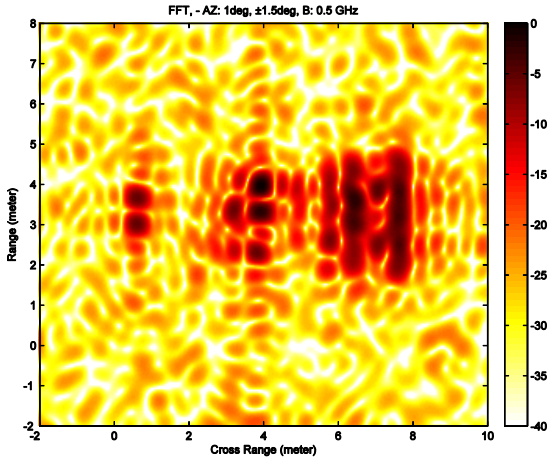

Fig. 22 2-D SAR image obtained from the Backhoe data set with SNR=5 dB via FFT algorithm

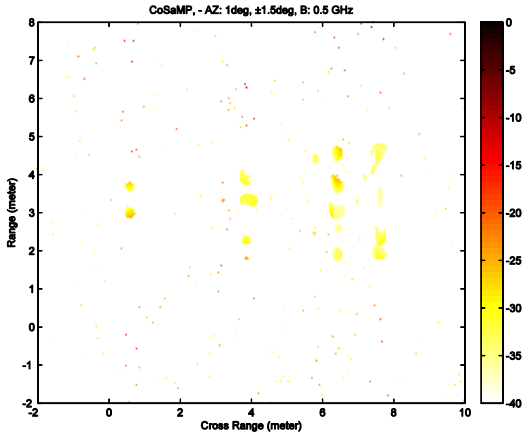

Fig. 23 2-D SAR image obtained from the Backhoe data set with SNR=5 dB via CoSaMP algorithm

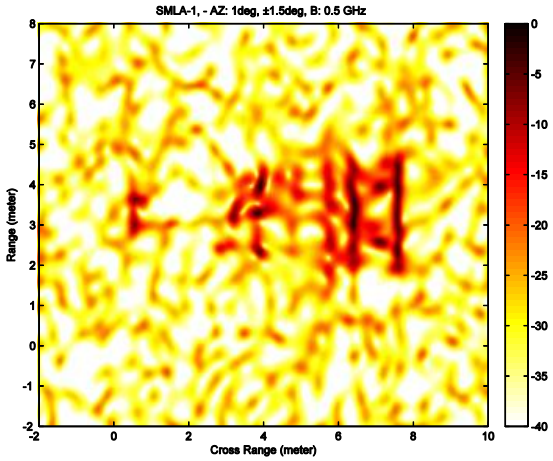

Fig. 24 2-D SAR image obtained from the Backhoe data set with SNR=5 dB via SMLA-1 algorithm

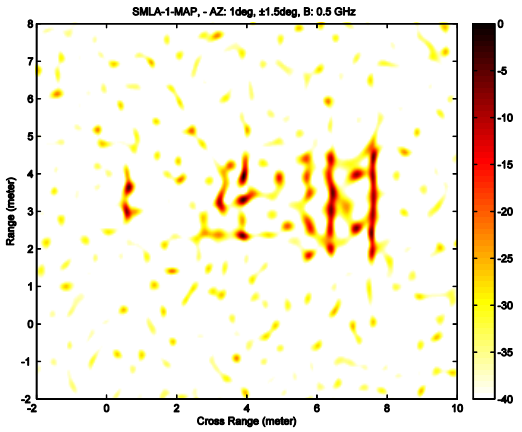

Fig. 25 2-D SAR image obtained from the Backhoe data set with SNR=5 dB via SMLA-1-MAP algorithm

C. SAR Images of the Gotcha Data

We illustrate here the application of SMLA-1-MAP, which has the best performance in the aforementioned numerical examples, to circular SAR imaging using the GOTCHA Air Force Research laboratory data set.

The GOTCHA dataset, Volumetric SAR Data Set, Version 1.0, consists of SAR phase history data collected at X-band with a 640 MHz bandwidth with full azimuth coverage at eight different elevation angles and full polarization [30]. The imaging scene consists of numerous civilian vehicles and calibration targets, as shown in Figs. 26-27. Imaging on a small area of the illuminated scene may be of more interest in practical applications. Below, we aim to reconstruct the image of a Chevrolet Malibu in the parking lot from the phase history data with full azimuth coverage collected at the first pass for a HH polarization channel.

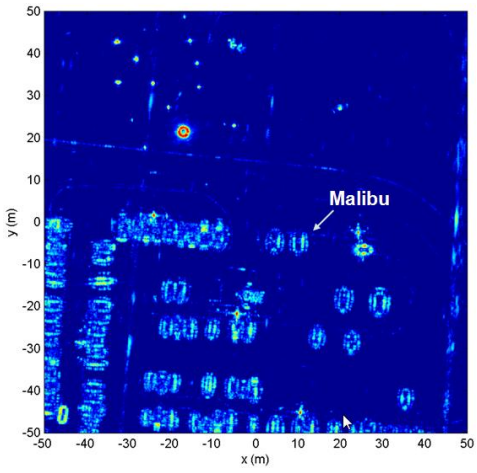

Fig. 26 2-D SAR image of the GOTCHA scene, from [30]

Fig. 27 Photograph of Chevrolet Malibu from the GOTCHA scene, from [30]

We use 4° subapertures from 0° to 360° with no overlap, which results in a total of 90 subapertures. For each subaperture, one 2D spatial image is formed by using a 2D FFT operation on the corresponding phase history (k-space) data. An 80×80 block of the spatial data centered about the Chevrolet Malibu is then chipped out and transformed back into k-space using an inverse FFT (IFFT) operation.

Different spectral analysis algorithms can be applied to the so-obtained 80×80 phase history data to get one image for each subaperture. With the help of the auxiliary information (e.g., the antenna locations, range to scene center, azimuth and elevation angles) provided by the GOTCHA data set, each image is then projected onto the ground plane and interpolated to form a 2D ground image. Finally, all of the 90 2D ground images are combined using the noncoherent max magnitude operator to yield the reconstructed Malibu image, whose dimensions are $[5,15]\times[-10,0]$ meters with a grid size of 0.05 meters in both dimensions.

Figs. 28-31 shows the reconstructed Chevrolet Malibu SAR images obtained by FFT, SMLA-1, SMLA-1-MAP and SLIM-1. Again, FFT has low resolution and high sidelobe problems, with the front portion of the vehicle mixed in with the background, as can be seen from Fig. 28. The Malibu image obtained by SMLA-1 is shown in Fig. 29.

In comparison, we can find that SMLA-1 provides significantly higher resolution and lower sidelobe level than FFT. The Malibu image obtained via SMLA-1-MAP is illustrated in Fig. 30, from which we can observe that the MAP step effectively converts the original dense Malibu images formed by SMLA-1 into a much sparser one. The Malibu image obtained by SLIM-1 is shown in Fig. 31.

We observe that the image formed by the SMLA-1-MAP is sparser than that of SLIM-1. It appears that the SMLA-1-MAP satisfactorily balances the tradeoffs between the image resolution (note that the SMLA-1-MAP outperforms SLIM-1 in terms of resolution) and detail preservation. We conclude that the user parameter-free SMLA-1-MAP again has the best performance.

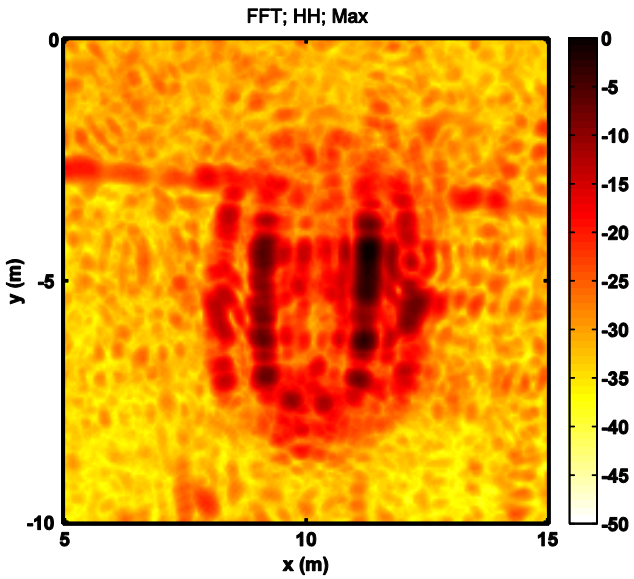

Fig. 28 2-D Malibu image obtained via FFT algorithm

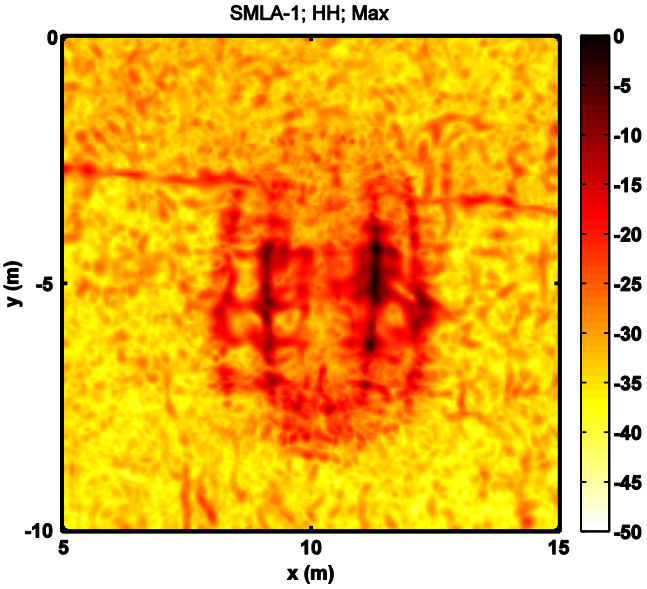

Fig. 29 2-D Malibu image obtained via SMLA-1 algorithm

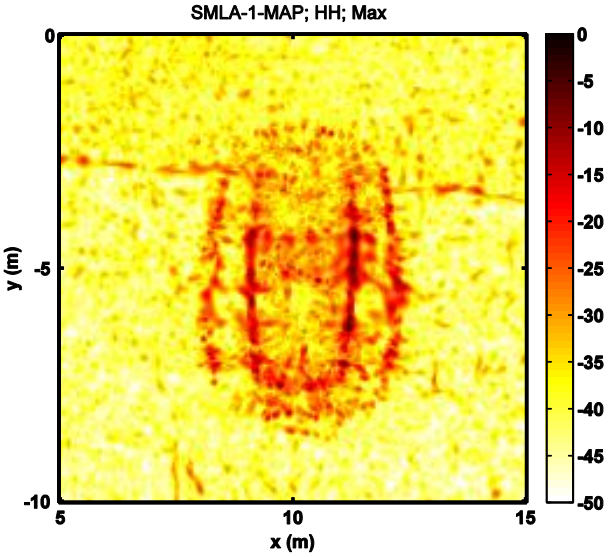

Fig. 30 2-D Malibu image obtained via SMLA-1-MAP algorithm

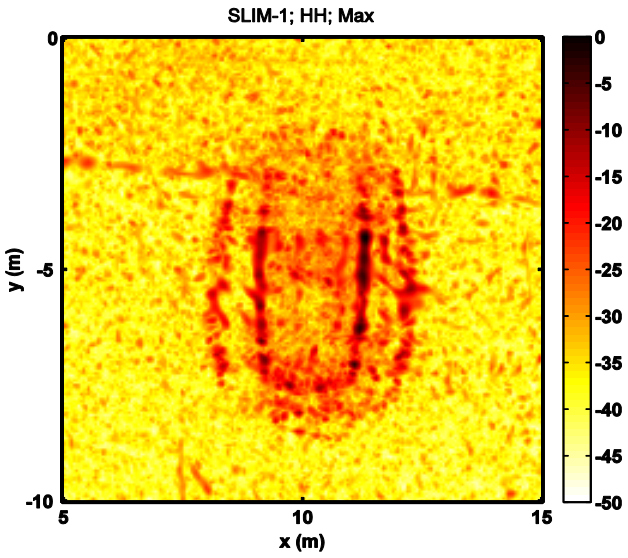

Fig. 31 2-D Malibu image obtained via SLIM algorithm

VII. CONCLUSIONS

We have presented a series of power-based iterative SMLA approaches for the SAR imaging application based on minimizing the SML criterion. Moreover, by exploiting the complex-valued nature of the SAR imaging problem, we have developed the SMLA-MAP approach, which combines a SMLA variant with the MAP approach. Both SMLA and SMLA-MAP approaches are user parameter free, making them easy to use in practice. Numerical and experimental results on various SAR imaging examples demonstrate the merit of the SMLA-MAP approach, which provides enhanced resolution and suppressed sidelobe levels compared to its SMLA counterpart and existing approaches. Among all the competing approaches, the newly proposed SMLA-1-MAP offers superior performance in terms of both SAR imaging quality and robustness against the presence of noise.

APPENDIX A

PROOF OF RESULT 1

Define the covariance matrix of the interference and noise as

$$\mathbf{Q}_k \overset{\text{def}}{=} \mathbf{R} - p_k \mathbf{a}_k \mathbf{a}_k^H. \tag{29}$$

Applying the matrix inversion lemma, we obtain

$$\mathbf{R}^{-1} = \mathbf{Q}_k^{-1} - p_k \beta_k \mathbf{b}_k \mathbf{b}_k^H, \tag{30}$$

where $\mathbf{b}_k \overset{\text{def}}{=} \mathbf{Q}_k^{-1}\mathbf{a}_k$ and $\beta_k \overset{\text{def}}{=} (1 + p_k \mathbf{a}_k^H \mathbf{Q}_k^{-1}\mathbf{a}_k)^{-1}$. Since

$$\mathbf{y}^H \mathbf{R}^{-1} \mathbf{y} = \mathbf{y}^H \mathbf{Q}_k^{-1} \mathbf{y} - p_k \beta_k \, |\mathbf{b}_k^H \mathbf{y}|^2, \tag{31}$$

$$\begin{aligned} \ln(\det(\mathbf{R})) &= \ln(\det(\mathbf{Q}_k + p_k \mathbf{a}_k \mathbf{a}_k^H)) \\ &= \ln\left[(1 + p_k \mathbf{a}_k^H \mathbf{Q}_k^{-1} \mathbf{a}_k)\det(\mathbf{Q}_k)\right] \\ &= \ln(\det(\mathbf{Q}_k)) - \ln(\beta_k), \end{aligned} \tag{32}$$

where we have used the well-known algebraic identity $\det(\mathbf{I} + \mathbf{AB}) = \det(\mathbf{I} + \mathbf{BA})$. By using a (31) and (32), the ML function (2) becomes

$$\ell(\mathbf{p}) = \ln(\det(\mathbf{Q}_k)) + \mathbf{y}^H \mathbf{Q}_k^{-1} \mathbf{y} - \left[\ln(\beta_k) + p_k \beta_k \, |\mathbf{b}_k^H \mathbf{y}|^2\right].$$

Consequently, minimizing (2) w.r.t. p_k is equivalent to minimizing the following function

$$\ell'(p_k) \overset{\text{def}}{=} \ln(1 + p_k \mathbf{a}_k^H \mathbf{Q}_k^{-1} \mathbf{a}_k) - p_k \beta_k \, |\mathbf{b}_k^H \mathbf{y}|^2, \tag{33}$$

where $\mathbf{Q}_k$ is assumed known and independent of p_k.

Note that (33) can be obtained from [22, Eq. (16)] derived for a multi-snapshot case by assuming $\mathbf{\Gamma} = \mathbf{y}\mathbf{y}^H$. Consequently, from [22, Appendix, Eqs. (27) and (28)], the unique minimizer of (33) is given by

$$\hat{p}_k = \frac{\mathbf{a}_k^H \mathbf{Q}_k^{-1} (\mathbf{y}\mathbf{y}^H - \mathbf{Q}_k) \mathbf{Q}_k^{-1} \mathbf{a}_k}{(\mathbf{a}_k^H \mathbf{Q}_k^{-1} \mathbf{a}_k)^2}. \tag{34}$$

Using (30), we have

$$\mathbf{a}_k^H \mathbf{Q}_k^{-1} \mathbf{a}_k = \gamma_k (\mathbf{a}_k^H \mathbf{R}^{-1} \mathbf{a}_k), \tag{35}$$

and

$$\alpha_k^H \mathbf{Q}_k^{-1} \mathbf{y} = \gamma_k^2 (\mathbf{a}_k^H \mathbf{R}^{-1} \mathbf{y}), \tag{36}$$

where $\gamma_k \overset{\text{def}}{=} 1 + p_k \mathbf{a}_k^H \mathbf{Q}_k^{-1} \mathbf{a}_k$. Substituting (35) and (36) into (34), we obtain the desired expression

$$\begin{aligned} \hat{p}_k &= \frac{\mathbf{a}_k^H \mathbf{R}^{-1} (\mathbf{y}\mathbf{y}^H - \mathbf{R}) \mathbf{R}^{-1} \mathbf{a}_k}{(\mathbf{a}_k^H \mathbf{R}^{-1} \mathbf{a}_k)^2} + p_k \\ &= \frac{|\mathbf{a}_k^H \mathbf{R}^{-1} \mathbf{y}|^2}{(\mathbf{a}_k^H \mathbf{R}^{-1} \mathbf{a}_k)^2} + p_k - \frac{1}{\mathbf{a}_k^H \mathbf{R}^{-1} \mathbf{a}_k}. \end{aligned} \tag{37}$$

Differentiating (2) with respect to σ and setting the result to zero, we obtain

$$\hat{\sigma} = \frac{\mathrm{Tr}(\mathbf{R}^{-1}(\mathbf{y}\mathbf{y}^H - \overline{\mathbf{R}})\mathbf{R}^{-1})}{\mathrm{Tr}(\mathbf{R}^{-2})},$$

and after substituting $\mathbf{R} - \sigma\mathbf{I}$ for $\overline{\mathbf{R}}$ in the above equation,

$$\begin{aligned} \hat{\sigma} &= \frac{\mathrm{Tr}(\mathbf{R}^{-1}(\mathbf{y}\mathbf{y}^H - \mathbf{R})\mathbf{R}^{-1})}{\mathrm{Tr}(\mathbf{R}^{-2})} + \sigma \\ &= (\mathbf{y}^H \mathbf{R}^{-2} \mathbf{y})/\mathrm{Tr}(\mathbf{R}^{-2}) + \sigma - \mathrm{Tr}(\mathbf{R}^{-1})/\mathrm{Tr}(\mathbf{R}^{-2}). \end{aligned}$$

Computing $\hat{p}_k$ and $\hat{\sigma}$ requires the knowledge of p_k, σ, and $\mathbf{R}$. Therefore the algorithm must be implemented iteratively as shown in Result 1.

APPENDIX B

PROOF OF RESULT 2

Differentiating (16) w.r.t. p_k and setting the result to zero, we get (after some simplification)

$$p_k^{(i+1)} = \frac{\bar{\mathbf{a}}_k^H \mathbf{C}_k'^{-1} \mathbf{r}_y}{\bar{\mathbf{a}}_k^H \mathbf{C}_k'^{-1} \bar{\mathbf{a}}_k}. \tag{38}$$

Applying the inversion lemma to the matrix $\mathbf{C}'_k$, the numerator and denominator of Eq. (38) , respectively, can be expressed as

$$\bar{\mathbf{a}}_k^H \mathbf{C}_k'^{-1} \mathbf{r}_y = w_k (\bar{\mathbf{a}}_k^H \mathbf{C}_r^{-1} \mathbf{r}_y), \tag{39}$$

and

$$\bar{\mathbf{a}}_k^H \mathbf{C}_k'^{-1} \bar{\mathbf{a}}_k = w_k (\bar{\mathbf{a}}_k^H \mathbf{C}_r^{-1} \bar{\mathbf{a}}_k), \tag{40}$$

where $w_k \overset{\text{def}}{=} 1 + \dfrac{\bar{\mathbf{a}}_k^H \mathbf{C}_r^{-1} \bar{\mathbf{a}}_k}{1/p_k^2 + \bar{\mathbf{a}}_k^H \mathbf{C}_r^{-1} \bar{\mathbf{a}}_k}$.

Thus,

$$p_k^{(i+1)} = \frac{\bar{\mathbf{a}}_k^H \mathbf{C}_k'^{-1} \mathbf{r}_y}{\bar{\mathbf{a}}_k^H \mathbf{C}_k'^{-1} \bar{\mathbf{a}}_k} = \frac{\bar{\mathbf{a}}_k^H \mathbf{C}_r^{-1} \mathbf{r}_y}{\bar{\mathbf{a}}_k^H \mathbf{C}_r^{-1} \bar{\mathbf{a}}_k}, \quad k = 1, \ldots, K+1. \quad (41)$$

Using the following identities (see e.g., [29, Th. 7.7, 7.16]),

$$\text{vec}(\mathbf{ABC}) = (\mathbf{C}^T \otimes \mathbf{A})\text{vec}(\mathbf{B}),$$

$$(\mathbf{A} \otimes \mathbf{B}) \otimes (\mathbf{C} \otimes \mathbf{D}) = \mathbf{AC} \otimes \mathbf{BD},$$

the nominator and denominator of Eq. (41) can be expressed, respectively, as

$$\bar{\mathbf{a}}_k^H \mathbf{C}_r^{-1} \mathbf{r}_y = |\mathbf{a}_k^H \mathbf{R}^{-1} \mathbf{y}|^2, \quad k = 1, \ldots, K, \quad (42)$$

and

$$\bar{\mathbf{a}}_k^H \mathbf{C}_r^{-1} \bar{\mathbf{a}}_k = (\mathbf{a}_k^H \mathbf{R}^{-1} \mathbf{a}_k)^2, \quad k = 1, \ldots, K, \quad (43)$$

and also

$$\bar{\mathbf{a}}_{K+1}^H \mathbf{C}_r^{-1} \mathbf{r}_N = \mathbf{y}^H \mathbf{R}^{-2} \mathbf{y}, \quad (44)$$

and

$$\bar{\mathbf{a}}_{K+1}^H \mathbf{C}_r^{-1} \bar{\mathbf{a}}_{K+1} = \text{Tr}(\mathbf{R}^{-2}). \quad (45)$$

Hence, the result of dividing (42) by (43) gives (11), and the result of dividing (44) by (45) gives (12).

APPENDIX C
PROOF OF THE KEY EQUALITY

Since $\mathbf{x}_{MAP} = \mathbf{P}\,\mathbf{A}^H \mathbf{R}^{-1} \mathbf{y}$, we have

$$\mathbf{x}_{MAP}^H \mathbf{P}^{-1} \mathbf{x}_{MAP} = \mathbf{y}^H \mathbf{R}^{-1} \mathbf{A}\mathbf{P}\,\mathbf{A}^H \mathbf{R}^{-1} \mathbf{y}, \quad (46)$$

and

$$\mathbf{y} - \mathbf{A}\mathbf{x}_{MAP} = (\mathbf{I} - \mathbf{A}\mathbf{P}\,\mathbf{A}^H \mathbf{R}^{-1}) \mathbf{y}. \quad (47)$$

Then,

$$\| \mathbf{y} - \mathbf{A}\mathbf{x}_{MAP} \|^2 = (\mathbf{y} - \mathbf{A}\mathbf{x}_{MAP})^H (\mathbf{y} - \mathbf{A}\mathbf{x}_{MAP}) \quad (48)$$

$$= \mathbf{y}^H (\mathbf{I} - \mathbf{R}^{-1} \mathbf{A}\mathbf{P}\,\mathbf{A}^H)(\mathbf{I} - \mathbf{A}\mathbf{P}\,\mathbf{A}^H \mathbf{R}^{-1}) \mathbf{y}.$$

The left hand side of (26) $\frac{1}{\sigma} \| \mathbf{y} - \mathbf{A}\mathbf{x}_{MAP} \|^2 + \mathbf{x}_{MAP}^H \mathbf{P}^{-1} \mathbf{x}_{MAP}$ is equal to

$$\mathbf{y}^H [\frac{1}{\sigma} (\mathbf{I} - \mathbf{R}^{-1} \mathbf{A}\mathbf{P}\,\mathbf{A}^H)(\mathbf{I} - \mathbf{A}\mathbf{P}\,\mathbf{A}^H \mathbf{R}^{-1}) + \mathbf{R}^{-1} \mathbf{A}\mathbf{P}\,\mathbf{A}^H \mathbf{R}^{-1}] \mathbf{y}. \quad (49)$$

If the inside part of the bracket is equal to $\mathbf{R}^{-1}$, then we are done.

Since

$$\frac{1}{\sigma} (\mathbf{I} - \mathbf{R}^{-1} \mathbf{A}\mathbf{P}\,\mathbf{A}^H)(\mathbf{I} - \mathbf{A}\mathbf{P}\,\mathbf{A}^H \mathbf{R}^{-1})$$

$$= \mathbf{R}^{-1} [\frac{1}{\sigma} (\mathbf{R} - \mathbf{A}\mathbf{P}\,\mathbf{A}^H)(\mathbf{R} - \mathbf{A}\mathbf{P}\,\mathbf{A}^H)] \mathbf{R}^{-1}$$

$$= \mathbf{R}^{-1} [\sigma \mathbf{I}] \mathbf{R}^{-1}, \quad (50)$$

the expression (49) becomes

$$\mathbf{y}^H [\mathbf{R}^{-1} (\sigma \mathbf{I} + \mathbf{A}\mathbf{P}\,\mathbf{A}^H) \mathbf{R}^{-1}] \mathbf{y} = \mathbf{y}^H [\mathbf{R}^{-1} (\mathbf{R}) \mathbf{R}^{-1}] \mathbf{y} = \mathbf{y}^H \mathbf{R}^{-1} \mathbf{y}. \quad (51)$$

REFERENCES

[1] C. V. Jakowatz, Jr. D. E. Wahl, P. H. Eichel, D. C. Ghiglia, and P. A. Thompson, Spotlight-Mode Synthetic Aperture Radar: A Signal Processing Approach., Norwell, MA: Kluwer Academic Publishers, 1996.

[2] W. G. Carrara, R. S. Goodman, and R. M. Majewski, *Spotlight synthetic aperture radar: Signal processing algorithms*, Norwood, MA, Artech House, 1995.

[3] J. Walker, ``Range-Doppler imaging of rotating objects," *IEEE Trans. Aerosp. Electron. Syst.*, vol. AES-16, pp. 23--52, Jan. 1980.

[4] D. C. Munson, Jr., J. D. O'Brien, and W. K. Jenkins, ``A tomographic formulation of spotlight-mode synthetic aperture radar," *Proc. IEEE*, vol. PROC-71, pp. 917-925, Aug. 1983.

[5] M. D. Desai and W. K. Jenkins, ``Convolution backprojection image reconstruction for spotlight mode synthetic aperture radar," *IEEE Trans. Image Processing*, vol. 1, pp. 505-517, Oct. 1992.

[6] J. Capon, ``High resolution frequency-wavenumber spectrum analysis," *Procedings of the IEEE* , vol. 57, pp. 1408-1418, August 1969.

[7] J. Li and P. Stoica, ``An adaptive filtering approach to spectral estimation and SAR imaging," *IEEE Transactions on Signal Processing*, vol. 44, pp. 1469--1484, June, 1996.

[8] S. R. DeGraaf, ``Sidelobe Reduction via Adaptive FIR Filtering in SAR Imagery," *IEEE Transactions on Image Processing*, vol. 3, pp. 292-301, May, 1994.

[9] S. R. DeGraaf, ``SAR Imaging via Modern 2-D Spectral Estimation Methods," *IEEE Transactions on Image Processing*, vol. 7, pp. 729-761, May, 1998.

[10] G. R. Benitz, ``High definition vector imaging for synthetic aperture radar," *31st Asilomar Conference on Signals, Systems and Computers*, Pacific Grove, CA, November, 1997.

[11] M. Cetin and W. C. Karl, ``Feature-enhanced synthetic aperture radar image formation based on nonquadratic regularization," *IEEE Transactions on Image Processing*, vol. 10, no. 4, pp. 623-631, Apr. 2001.

[12] S. Samadi, M. Cetin and M. A. Masnadi-Shirazi, ``Sparse representation-based synthetic aperture radar imaging," *IET Radar Sonar Navig.*, vol. 5, no. 2, pp. 182-193, 2011.

[13] T. J. Kragh and A. A. Kharbouch, ``Monotonic Iterative Algorithms for SAR Image Restoration," *Proceedings of the International Conference on Image Processing*, Atlanta, GA, October, 2006.

[14] D. Needell and J. A. Tropp, ``CoSaMP: Iterative signal recovery from incomplete and inaccurate samples," *Appl. Comp. Harmonic Anal.*, vol. 26, pp. 301-321. May 2009.

[15] X. Tan, W. Roberts, J. Li, and P. Stoica, ``Sparse learning via iterative minimization with application to MIMO radar imaging," *IEEE Trans. Signal Process.*, vol. 59, no. 3, pp. 1088-1101, March 2011.

[16] D. Wipf, B. D. Rao, and S. Nagarajan, ``Latent variable Bayesian models for promoting sparsity," *IEEE Trans. on Information Theory*, vol. 57, no. 9, pp. 6236-6255, Sept. 2011.

[17] D. Wipf and S. Nagarajan, ``A new view of automatic relevance determination," *in Proc. Adv. Neural Inf. Process. Syst.*, pp. 1625-1632, 2008.

[18] R. Chartrand and W. Yin, ``Iteratively reweighted algorithms for compressive sensing," *In ICASSP 2008*, pp. 3869-3872, March 2008.

[19] D. J. Andersh, M. Hazlett, S. W. Lee, D. D. Reeves, D. P. Sullivan, and Y. Chu,``XPATCH: a high-frequency electromagnetic scattering prediction code and environment for complex three-dimensional objects," *IEEE Antennas and Prop. Magazine*, vol. 36, pp. 65-69, Feb. 1994.

[20] W. Roberts, P. Stoica, J. Li, T. Yardibi, and F. A. Sadjadi, ``Iterative adaptive approaches to MIMO radar imaging," *IEEE Journal on Selected Topics in Signal Proc.*, vol. 4, no. 1, pp. 5-20, 2010.

[21] Z. Chen, X. Tan, M. Xue, and J. Li, ``Bayesian SAR imaging," *In Proc. of SPIE on Technologies and Systems for Defense and Security*,, Orlando, FL, April 2010.

[22] T. Yardibi, J. Li, P. Stoica, M. Xue, and A. B. Baggeroer, ``Source localization and sensing: A nonparametric iterative adaptive approach

based on weighted least squares," *IEEE Trans. Aerosp. Electron. Syst.*, vol. 46, pp. 425-443, 2010.

[23] G.-O. Glentis and A. Jakobsson, ``Efficient implementation of iterative adaptive approach spectral estimation techniques," *IEEE Transactions on Signal Processing*, vol. 59, no. 9, pp. 4154-4167, Sept. 2011.

[24] M. Xue, L. Xu, and J. Li, ``IAA spectral estimation: Fast implementation using the Gohberg-Semencul factorization," *IEEE Transactions on Signal Processing*, vol. 59, no. 7, pp. 3251-3261, July 2011.

[25] D. Vu, L. Xu, M. Xue, and J. Li, ``Nonparametric missing sample spectral analysis and its applications to interrupted SAR," *IEEE Journal of Selected Topics in Signal Processing*, to appear.

[26] P. Stoica, P. Babu, and J. Li, ``New method of sparse parameter estimation in separable models and its use for spectral analysis of irregularly sampled data," *IEEE Transactions on Signal Processing*, vol. 59, no. 1, pp. 35-47, 2011.

[27] T. M. Cover and J. A. Thomas, ``Determinant inequalities via information theory," *SIAM J. Matrix Anal.*, vol. 9, no. 3, pp. 384-392, July 1988.

[28] P. Stoica and R. Moses, *Spectral Analysis of Signals*, Upper Saddle River, NJ: Prentice-Hall, 2005.

[29] J. R. Schott, *Matrix Analysis for Statistics*, New York: Wiley, 1980.

[30] ``Gotcha 2D/3D imaging challenge problem," Air Force Research Lab., Jan.2010, Available: https://www.sdms.afrl.af.mil/datasets/gotcha/.

Habti Abeida was born in Settat, Morocco, on October 20, 1977. He received the B.Sc. degree in engineering applied mathematics from Hassan II University, Casablanca, Morocco, and Descartes University, Paris, France, in 2000 and 2001, respectively, and the M.S. degree in statistics and signal processing from Pierre and Marie Curie University, Paris, France, in 2002. He received the Ph.D. degree in signal processing and applied mathematics from Pierre and Marie Curie University, Paris, France, in collaboration with Telecom SudParis, France, in 2006. He was a Lecturer at the Paris-Dauphine and at the Vincennes-Saint-Denis Paris 8 University, in 2006 and 2007, respectively. He was a Postdoctoral Research Associate at the Superior school of electricity, Supelec, Paris, France, at the GIPAS-lab, Grenoble, France, at the Electrical Engineering Department, KFUPM, Saudi Arabia, and at the spectral analysis laboratory, University of Florida, United States, in 2008, 2009, 2010, and 2011, respectively. He is currently working as an assistant professor at the Electrical Engineering Department, Taif University, Saudi Arabia. His research interests are in the areas of statistical signal processing with application to communications and antenna array.

Xianqi Li received B. Sc degree from Liaoning University, Shenyang, in 2007, and M.Sc. Degree from the University of Texas-Pan American, Edinburg, in 2009, both in Mathematics. He is currently pursuing the Ph. D degree with the Department of Electrical and Computer Engineering, University of Florida, Gainesville. His research interests are in the areas of statistical signal processing and image processing.

Jian Li (S'87-M'91-SM'97-F'05) received the M.Sc. and Ph.D. degrees in electrical engineering from The Ohio State University, Columbus, in 1987 and 1991, respectively. From April 1991 to June 1991, she was an Adjunct Assistant Professor with the Department of Electrical Engineering, The Ohio State University, and Columbus. From July 1991 to June 1993, she was an Assistant Professor with the Department of Electrical Engineering, University of Kentucky, and Lexington. Since August 1993, she has been with the Department of Electrical and Computer Engineering, University of Florida, Gainesville, where she is currently a Professor. In fall 2007, she was on sabbatical leave at MIT, Cambridge, Massachusetts. Her current research interests include spectral estimation, statistical and array signal processing, and their applications. Dr. Li is a Fellow of IEEE and a Fellow of IET. She is a member of Sigma Xi and Phi Kappa Phi. She received the 1994 National Science Foundation Young Investigator Award and the 1996 Office of Naval Research Young Investigator Award. She was an Executive Committee Member of the 2002 International Conference on Acoustics, Speech, and Signal Processing, Orlando, Florida, May 2002. She was an Associate Editor of the IEEE Transactions on Signal Processing from 1999 to 2005, an Associate Editor of the IEEE Signal Processing Magazine from 2003 to 2005, and a member of the Editorial Board of Signal Processing, a publication of the European Association for Signal Processing (EURASIP), from 2005 to 2007. She has been a member of the Editorial Board of the IEEE Signal Processing Magazine since 2010 and a member of the Editorial Board of Digital Signal Processing -- A Review Journal, a publication of Elsevier, since 2006. She is a co-author of the papers that have received the First and Second Place Best Student Paper Awards, respectively, at the 2005 and 2007 Annual Asilomar Conferences on Signals, Systems, and Computers in Pacific Grove, California. She is a co-author of the paper that has received the M. Barry Carlton Award for the best paper published in IEEE Transactions on Aerospace and Electronic Systems in 2005. She is also a co-author of the paper that has received the Lockheed Martin Best Student Paper Award at the 2009 SPIE Defense, Security, and Sensing Conference in Orlando, Florida.

Mosleh M. Al-Harthi was born in Taif, Saudi Arabia, on October 15, 1966. He received the B.Sc. degree in electronics technology and engineering from Indiana State University, Terre Haute, USA, in 1996, and the M.S. degree in electronics technology and engineering from Indiana State University, Terre Haute, USA, in 1997. He received the Ph.D. degree in electrical engineering from Arkansas University, Fayetteville, USA, in 2001. He was an assistant professor at College of Technology in Jeddah, Saudi Arabia form 2001 till 2009. He is currently working as an associate professor at the Electrical Engineering Department, Taif University, Saudi Arabia. His research interests are in the areas of control engineering, electronics, and signal processing.